Gaussian Process Regression with Automatic Relevance Determination Kernel for Calendar Aging Prediction of Lithium-ion Batteries

Kailong Liu, *Member, IEEE*, Yi Li, Xiaosong Hu, *Senior member, IEEE*,
Mattin Lucu and Widanalage Dhammika Widanage, *Member, IEEE*,

Abstract—Battery calendar aging prediction is of extreme importance for developing durable electric vehicles. This paper derives machine learning-enabled calendar aging prediction for lithium-ion batteries. Specifically, the Gaussian process regression (GPR) technique is employed to capture the underlying mapping among capacity, storage temperature, and SOC. By modifying the isotropic kernel function with an automatic relevance determination (ARD) structure, high relevant input features can be effectively extracted to improve prediction accuracy and robustness. Experimental battery calendar aging data from nine storage cases are utilized for model training, validation, and comparison, which is more meaningful and practical than using the data from a single condition. Illustrative results demonstrate that the proposed GPR model with ARD Matern32 (M32) kernel outperforms other counterparts and can achieve reliable prediction results for all storage cases. Even for the partial-data training test, multi-step prediction test and accelerated aging training test, the proposed ARD-based GPR model is still capable of excavating the useful features, therefore offering good generalization ability and accurate prediction results for calendar aging under various storage conditions. This is the first known data-driven application that utilizes the GPR with ARD kernel to perform battery calendar aging prognosis.

Index Terms—Lithium-ion batteries, calendar aging prediction, battery health, Gaussian process regression, data-driven model.

I. INTRODUCTION

Lithium-ion (Li-ion) batteries are the promising candidates for electric vehicle (EV) applications, owing to their impressive features such as high energy density, high efficiency

K. Liu and W. D. Widanage are with the Warwick Manufacturing Group, University of Warwick, Coventry, CV4 7AL, United Kingdom (e-mails: Kailong.Liu@warwick.ac.uk, kliu02@qub.ac.uk; Dhammika.Widanalage@warwick.ac.uk).
Y. Li is with the Department of Chemistry, Lancaster University, Lancaster, LA1 4YB, United Kingdom (e-mail: y.li82@lancaster.ac.uk).
X. Hu is with the Department of Automotive Engineering, Chongqing University, Chongqing, 400044, China (e-mail: xiaosonghu@ieee.org).
Mattin Lucu is with the IK4-Ikerlan Technology Research Centre and the University of the Basque Country, Spain (e-mail: mlucu@ikerlan.es).

and environmental friendliness [1]. However, reliable calendar aging prediction is still a bottleneck for the performance enhancement of EVs. In real automotive applications, Li-ion batteries generally degrade with the calendar and cyclic modes. Considering that more than 75% of battery life is spent under parking mode for EVs [2], calendar aging prediction therefore becomes a prerequisite for battery service life diagnosis.

Calendar aging for most Li-ion batteries is mainly caused by the growth of solid electrolyte interface (SEI) during storage [3]. Specifically, when a battery is stored, the reduction of its electrolyte solvents such as ethylene carbonate would cause the formation of Li-based products, further resulting in the generation of SEI on the anode particle of battery [4]. In such cases, Li-ion battery capacity would decrease over time [5]. The corresponding capacity aging rate is highly dependent on several key factors including the storage temperature and battery state-of-charge (SOC) [6]. Therefore, a key but challenging issue for calendar aging prediction is to simultaneously take these factors into account. It is vital to develop suitable models to capture capacity degradation dynamics under various storage conditions.

Several physics-based models have been reported in the literature to explain battery calendar aging behaviors [7], [8]. Although electrochemical dynamics of batteries during storage have been analysed in the simulation environment, these models are highly time-consuming and complex to parametrise, making them overly expensive for real-time calendar aging prediction on a long period scale.

To overcome the above challenges, calendar aging prediction approaches based on semi-empirical models have been designed. For instance, Schmalstieg et al. [9] proposed an Arrhenius-based semi-empirical model to capture calendar cell aging. Petit et al. [10] developed an empirical capacity loss model to evaluate the effects of SOC and temperature on storage lifetime of Li-ion batteries. In [11], instead of using Arrhenius acceleration model, a semi-empirial approach based on the Eyring acceleration model was adopted to predict battery calendar aging, while the SOC drifting was also taken into account. By considering the effects of temperature and storage conditions, De Hoog et al. [12] proposed a semi-empirical combined model to estimate the calendar lifetime for a Nickel-manganese-Cobalt Oxide battery. In [13], by taking the initial surface layer caused by cell formation into account, an extended semi-empirical model was proposed to improve

the calendar aging predictive ability. These referred works belong to open-loop models without strong generalization abilities, in a way, their performance highly depend on the quality of test experiments.

Data-driven models, which are free of assuming any mechanism a priori, are also gaining increasing attention in the battery state-of-health (SOH) estimation and remaining useful life diagnosis [14]. Different intelligent techniques such as support vector regression [15], [16], Bayesian prediction [17], [18], and artificial neural network [19]–[21] have been successfully applied to build data-driven models for battery cyclic aging prediction. On the one hand, some review papers have summarised these state-of-the-art applications [22], [23], concluding that several limitations still exist as: 1) data-driven approaches are mainly used to capture battery cyclic aging states but very few attempts have been done for calendar aging diagnosis. 2) most publications fit the model on aging data obtained under constant operating conditions, ignoring various cases of temperature and SOC. Such models are infeasible for predicting capacity under different conditions. On the other hand, in a previous publication, a critical review on various data-driven models in battery aging domain was presented, in which the Gaussian process regression (GPR) is identified as one most powerful technique. Detailed comparisons for different machine learning techniques are referred to the Table 5 of [14] and the corresponding discussions. In fact, beyond the performance of simple structure and computationally acceptable predictions, GPRs enjoy the significant merits of being non-parametric and able to consider the uncertainty of predicted values. Through formulating specific input features, GPR-based models have been applied successfully in both academic and industrial domains [24]–[26]. However, to the best of our knowledge, there is still a lack of researches by using GPR in battery calendar aging prediction domain.

Besides, most existing works just use single conventional kernels to develop their GPR techniques without considering the correlations of multi-dimensional input variables. In the light of this, it could be a promising way through developing an improved GPR technique with the multi-dimensional kernel structure to capture the battery capacity degradation dynamics under different temperature and SOC storage conditions.

Based on the above discussions, this paper is concerned with machine learning-enabled calendar aging prediction for Li-ion batteries, where both the corresponding storage temperature and battery SOC can be taken into account simultaneously. Several key original contributions are made in this study. First, nine cases of experimental calendar aging data are collected under various storage temperatures and SOC levels over 480 days, constituting a well-rounded database to train and validate the calendar aging model. Second, because the battery calendar aging involving local fluctuations over storage time is a highly nonlinear process, a framework based on the GPR model is proposed to efficiently capture the capacity degradation dynamics with reliable confidence ranges. Third, due to the input features involving storage temperature and cell SOC, the isotropic kernel function of GPR is modified with an automatic relevance determination (ARD) structure, which brings the benefits that irrelevant inputs can be removed by
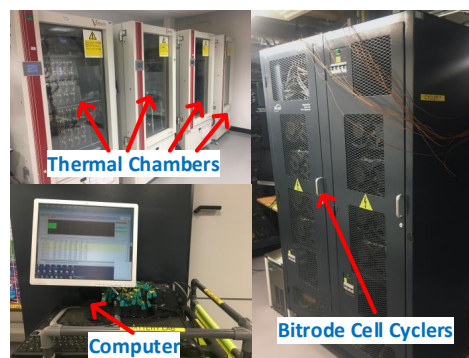

Fig. 1. Calendar aging test equipment.

fixing large length scales. Meanwhile, various predictors can be formulated to improve prediction accuracy and robustness. Finally, based upon our dataset, the prediction performance of our proposed GPR model is investigated in terms of different kernel functions, and compared with a regression calendar-life (RCL) model. This is the first known data-driven application by utilizing GPR with ARD kernel to handle battery calendar aging predictions. Obviously, due to mechanism-free characteristics, the proposed GPR+ARD model can be readily extendable to other battery types for calendar aging prognosis.

The rest of this paper is outlined as follows. Section II presents the calendar aging experiments and the collected dataset. Section III introduces the developed model framework and several key quantitative metrics, followed by the description of ARD-based GPR model. Section IV analyzes the comparison and verification results. Finally, Section V summaries this study.

II. CALENDAR AGING TEST

Fig. 1 illustrates the equipment used for conducting the battery calendar aging tests under different conditions. The cells were stored in the Votsch VT3050 Thermal Chambers, and operated by the Bitrode MVC 16-100-5 Cell Cyclers. The generated battery data were monitored and stored by a computer. Commercial Panasonic NCRBD batteries from a commercial automotive company were the cells used to study calendar aging characteristics of Li-ion batteries. The battery has a 3Ah nominal capacity, 2.5V lower cut-off voltage, and 4.2V upper cut-off voltage. Due to the rate of degradation can be minimized through keeping the SOC at a low or medium level and lowering the battery temperature [27], all cells are stored at 10^oC and moderate 50% SOC prior to any tests.

The calendar aging test was performed under various storage temperatures ($10^\circ C$, $25^\circ C$, and $45^\circ C$) and SOC levels (20%, 50%, and 90%) for a storage time of 480 days. All batteries were set in the temperature chambers with an open circuit status during storage. For each storage temperature and SOC, three cells were studied to obtain the average battery capacity and minimise any battery-to-battery discrepancies.

Periodic check-ups were performed every 30 days to obtain the capacity information during storage. For all tests, 1 C-rate is equal to 3A. At each check-up the temperature chambers

were set to $25°C$. Each cell was then charged by a constant-current constant-voltage (CC-CV) pattern with 1/2 C-rate in the CC phase until the terminal voltage reached 4.2V, followed by a CV phase until the current dropped below 1/10 C-rate. After resting for 3h, the cells were discharged by a CC pattern with 1/3 C-rate until the lower cut-off voltage of 2.5V. The average discharge capacity (over the three cells) was selected as the battery capacity for each condition. Before calibrating the SOC of cells, CC-CV pattern would be implemented again to recharge all batteries to their full-charging states. After another 3h rest period, the batteries were discharged to their specified SOC setpoints by a well-controlled coulomb counting method. Fig. 2 illustrates the open circuit voltage (OCV)-SOC curve for our adopted NCRBD battery. The OCV-SOC points at which the batteries were stored are also highlighted with red. Subsequently, each temperature chamber was readjusted to its specified storage condition again.
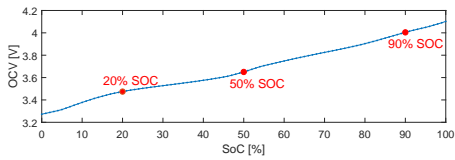

Fig. 2. OCV-SOC curve for the tested NCRBD battery.

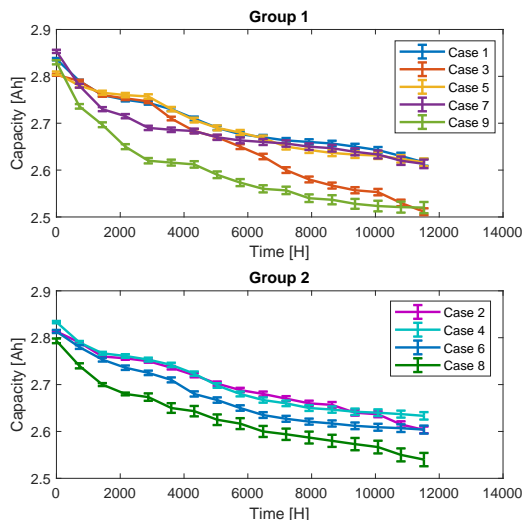Fig. 3. Calendar aging dataset for different storage conditions.

Fig. 4. Capacity degradations in calendar aging with standard deviations versus storage hours for different cases.

Following this procedure, the calendar aging dataset that contains nine storage cases was obtained, as shown in Fig. 3. Five cases (Case 1, Case 3, Case 5, Case 7 and Case 9) are labelled as 'Group 1' and another four cases (Case 2, Case 4, Case 6 and Case 8) are labelled as 'Group 2'. Detailed capacity aging curves with the standard deviations versus time for various storage conditions are illustrated in Fig. 4. Several of the capacity fade trends illustrate an initial rapid capacity fade followed by a more linear decrease. This phenomenon is attributed to the presence of excess anode electrode area in comparison to the cathode electrode area. Known as anode "overhang" in literature [28], [29], an outflow of Li-ions can occur from the active regions of the anode to its excess passive regions, leading to the initial rapid capacity fade. The subsequent linear capacity fade is then attributed to the irreversible capacity fade due to SEI growth.

The initial battery capacities C_{ini} for these cases are all different from each other, as described in Table I. It can be also seen that the initial measured capacities do not start from the nominal capacity of cell, which is a practical and likely scenario to occur.

TABLE I
INITIAL BATTERY CAPACITY VALUES FOR DIFFERENT CASES

Group 1	Case 1	Case 3	Case 5	Case 7	Case 9
C_{ini} [Ah]	2.837	2.802	2.807	2.852	2.830
Group 2	Case 2	Case 4	Case 6	Case 8	
C_{ini} [Ah]	2.812	2.833	2.813	2.794	

III. TECHNIQUE

This section elaborates the modelling methodology as well as the corresponding quantitative metrics. Additionally, the fundamentals of GPR technique with ARD kernel are presented, followed by a brief description of a regression calendar-life (RCL) model for comparison purposes.

A. Model development and quantitative metrics

On the basis of the tested calendar aging dataset, machine learning-based techniques can be developed to capture capacity degradation dynamics with various storage conditions. Compared with the existing data-driven models that normally consider just capacity information, an innovative model structure, which also takes both storage temperature term and battery SOC term into account, is developed for calendar aging prediction, as shown in Fig. 5. This model framework can be mainly divided into two parts. For the prediction of next capacity point, output $C_{sto}(t+1)$ can be predicted after using GPR to learn the underlying mappings among all input terms including the historical capacity data vector $[C_{sto}(t-k),...,C_{sto}(t)]$, storage SOC level SOC_{sto} and temperature T_{sto}. In GPR, these mappings are reflected within the covariance functions. Detailed pseudo-code of this mapping can be found in Section 2 of [30]. For the multi-step prediction, as illustrated in the green dashed line of Fig. 5, an iteration process that uses the previously predicted capacity as the next input to further predict new capacity value is
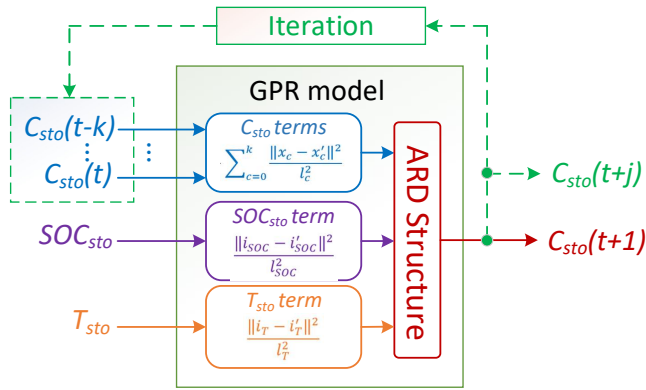
Fig. 5. Model framework for calendar aging prediction.

conducted until the jth capacity value is achieved. Here j and k represent the horizons of future and previous calendar capacities, respectively. In order to use our collected dataset and verify the prediction performance of proposed model, the capacity prediction in our study is conducted in steps of 30 days (720 hours) for a total time duration of 480 days (11520 hours). Through a trial-and-error method, the case of '$k = 2$' is selected due to a good trade-off between computational effort and prediction accuracy.

After constructing the proper input-target pairs from the battery calendar aging dataset, the GPR technique is employed to study the potential mapping mechanism, giving rise to the capacity prediction model that considers various storage conditions. Based upon our collected dataset as shown in Fig. 3, in order to ensure enough aging information can be learned for pure machine-learning techniques, the dataset from 'Group 1' (green cases) that covers all temperatures and SOCs, is applied for model training purpose. After training, the dataset from 'Group 2' (yellow cases) is used to verify the effectiveness of the proposed model.

Moreover, to evaluate the prediction performance of the data-driven model, several key quantitative metrics are adopted in this study [31]. Here N is the total number of predicted points, y_j and $\tilde{y}_j$ stand for each actual capacity data and each predicted value, respectively.

1) Maximum absolute error (MAE): By defining as (1), MAE is used to illustrate the maximum difference between the predicted and real test values. The larger the MAE values, the poorer the predicted accuracy is [31].

$$MAE = \max_{1 \le j \le n} |y_j - \tilde{y}_j|. \tag{1}$$

2) Root mean square error (RMSE): RMSE is another widely used metric to measure the overall difference between the predicted values and real test values. By defining as (2), the closer RMSE reaches to 0, the better the prediction accuracy is achieved [31].

$$RMSE = \sqrt{\frac{1}{N} \sum_{j=1}^{N} (y_j - \tilde{y}_j)^2}. \tag{2}$$

3) Fit-goodness (R^2): R^2 is defined by (3) to measure the match quality of a model to the real test data [32].

$$R^2 = 1 - \frac{\sum_{j=1}^{N} (y_j - \tilde{y}_j)^2}{\sum_{j=1}^{N} (y_j - \bar{y})^2}, \tag{3}$$

where $\bar{y}$ is the mean of the predicted values. It is evident that as R^2 approaches 1, the corresponding model well describes the variability of the target class.

4) Calibration score (CS): By defining as (4), CS reflects the frequency of real data lying within the obtained confidence range [24].

$$CS = \frac{1}{N} \sum_{j=1}^{N} [|y_j - \tilde{y}_j| < 2\sigma]_I, \tag{4}$$

where $[\cdot]_I$ represents the Iverson bracket. For a GPR model, 95.4% is a general confidence range with the interval corresponding to $\pm 2\sigma$ [24]. Therefore, the ideal CS should get close to 0.954: be less or larger than this value indicates that the developed model is over-confident or under-confident, respectively.

B. GPR technique with ARD kernel structure

Derived from the Bayesian framework, the GPR is able to undertake nonparametric regression with the Gaussian process. By defining the mean function $m(i)$ and covariance function $\kappa(i, i')$ of a real process $f(i)$ as:

$$\begin{cases} m(i) = \mathrm{E}\left(f(i)\right) \\ \kappa\left(i, i'\right) = \mathrm{E}\left[(m(i) - f(i))\left(m(i') - f(i')\right)\right] \end{cases}. \tag{5}$$

The probability distributions of GPR can be specified by [30]:

$$f(i) \sim GPR\left(m(i), \kappa\left(i, i'\right)\right). \tag{6}$$

Supposing that the same Gaussian distribution exists between the training set i and the new dataset i', then the corresponding output y' can be calculated by the conditional distribution as [24], [33]:

$$p\left(y' | i, y, i'\right) = N\left(y' | \bar{y}', \mathrm{cov}\left(y'\right)\right), \tag{7}$$

with

$$\begin{cases} \bar{y}' = \kappa(i, i')^T [\kappa(i, i)]^{-1} y \\ \mathrm{cov}(y') = \kappa(i', i') - \kappa(i, i')^T [\kappa(i, i)]^{-1} \kappa(i, i') \end{cases} \tag{8}$$

where y', $\bar{y}'$ and $cov(y')$ are the GPR posterior prediction, its corresponding mean and covariance, respectively. $N()$ indicates a normal distribution; $\kappa(i, i)$, $\kappa(i', i')$, and $\kappa(i, i')$ are the covariance matrices between just training inputs, just validation inputs, as well as training and validation inputs, respectively; y denotes the training output vector. It should be known that the uncertainty quantification of GPR in our study are actually the confidence boundaries to reflect the 'scope compliance' uncertainty of predicted values. This uncertainty is caused by differences between the modelled context and the application context, which is not the same as the standard deviations of measurements [30].

The performance of GPR is fully determined by its $m(i)$ and $\kappa(i, i')$, indicating that the corresponding kernel function must be selected and learned carefully from the training dataset. Among various kernel types, several simple but effective kernel functions are particularly noteworthy.

Squared-exponential (SE) function is a more widely used kernel function given as [30]:

$$\kappa_{SE}\left(i, i'\right) = \sigma_{SE}^2 \exp\left[\frac{-\left(i - i'\right)^2}{2l_{SE}^2}\right], \qquad (9)$$

where σ_{SE} and l_{SE} are hyperparameters to control the amplitude and length scales. To some extent, SE kernel belongs to a stationary-type kernel in that the correlations between different points are purely affected by the term $i - i'$, leading to a smooth distribution. This would be too strict for capacity degradation data with many local fluctuations, therefore an alternative is the Matern32 (M32) kernel function as [30]:

$$\kappa_{M32}\left(i, i'\right) = \sigma_{M32}^2 \left[1 + \frac{\sqrt{3}\left(i - i'\right)}{l_{M32}}\right] \exp\left[-\frac{\sqrt{3}\left(i - i'\right)}{l_{M32}}\right] \qquad (10)$$

where σ_{M32} and l_{M32} represent the hyperparameters to control the function amplitude and smoothness respectively.

In practice, due to the limited capture ability of the SE function and M32 function, these isotropic kernels would provide unreliable predictive results for nonlinear mapping that involves multidimensional input variables. For the calendar aging model, the inputs should not only contain the capacity terms, but also involve the storage temperature and cell SOC. In order to extract these features and improve accuracy, the isotropic SE and M32 kernels are modified with the ARD structure [34], as denoted by (11) and (12).

$$\begin{cases} \kappa_{SE\sim ARD}(i, i') = \sigma_{SE}^2 \exp[-\frac{1}{2}r] \\ \kappa_{M32\sim ARD}(i, i') = \sigma_{M32}^2(1 + \sqrt{3r}) \exp(-\sqrt{3r}) \end{cases}, \qquad (11)$$

with

$$r = \frac{\left\|i_T - i'_T\right\|^2}{l_T^2} + \frac{\left\|i_{SOC} - i'_{SOC}\right\|^2}{l_{SOC}^2} + \sum_{C=0}^{k} \frac{\left\|i_C - i'_C\right\|^2}{l_C^2} \qquad (12)$$

where hyperparameters l_T, l_{SOC} and l_C determine the relevancies of temperature, SOC and capacities inputs with respect to the regression results, respectively. Generally, a large value leads to a low relevancy. For GPR, the 'learning' implies to the optimization of hyperparameters within the covariance function, using the training dataset. In our study, a standard gradient descent optimizer is used to fit the hyperparameters of GPR through maximizing the log marginal likelihood [30]. Here the threshold of gradient descent optimizer is $2 \times e^{-5}$, which is defined by Matlab GPR toolbox.

Therefore, ARD structure can be seen as a powerful tool for input features extraction. By using the ARD kernel for calendar aging prediction, irrelevant input features among

TABLE II
IDENTIFIED PARAMETERS FOR RCL MODEL

Parameters	α_1	α_2	α_3	α_4	p
Values	0.0006	0.5270	-2.7049	-1.0185	0.52

capacity, storage temperature, and SOC would be effectively removed by fixing large length scales for them, yielding a sparse and explanatory subset of features. Besides, various predictors with different length scales are generated to improve prediction accuracy and robustness.

C. Regression calendar-life model

In order to demonstrate the effectiveness of the proposed GPR+ARD model, a simplified regression calendar-life (RCL) model is also adopted and compared. This RCL model is actually a typical semi-empirical model which has been applied in publication [11]. Generally, the capacity loss ΔQ during storage is expressed as a function of the battery SOC SOC_{sto}, storage temperature T_{sto}, and storage time duration t as [11]:

$$\Delta Q = f\left(SOC_{sto}, T_{sto}, t\right). \qquad (13)$$

Then (13) can be simplified by assuming decoupling. First, both battery SOC and T_s versus time, implying that the calendar degradation trend is similar over time and can be shaped by a coefficient as [11]:

$$\Delta Q = C\left(SOC_{sto}, T_{sto}\right) t^p. \qquad (14)$$

In the literature, the shaping coefficient $C(SOC_{sto}, T_{sto})$ is usually assumed to follow the Arrhenius relation, allowing the SOC_{sto} and T_{sto} to be decoupled as [11]:

$$C\left(SOC_{sto}, T_{sto}\right) = A(z) \exp\left[-\frac{E_a(SOC_{sto})}{kT_{sto}}\right]. \qquad (15)$$

It is noteworthy that the activation energy, denoted E_a in the (15), could be approximated by an affine linear dependence of SOC [11], as expressed in (16).

$$\Delta Q = \alpha_1 \exp\left[\alpha_2 \cdot SOC_{sto}\right] \exp\left[(\alpha_3 \cdot SOC_{sto} + \alpha_4)/T_{sto}\right] t^p. \qquad (16)$$

For this RCL model, input parameters include the storage SOC, temperature and time duration. Following the same datasets as GPR, all data from 'Group 1' (green cases) are used to train the RCL model, while all data from 'Group 2' (yellow cases) are used to validate the trained RCL model. In this study, five parameters (α_1, α_2, α_3, α_4 and p) require to be identified. An advanced heuristic method named biogeography-based optimization (BBO) is adopted to calculate these parameters by minimizing the RMSE between the predicted values and the real test data through 20 independent runs. More details regarding the BBO technique and the identification procedure can be found in [35]. The corresponding identified parameters are shown in Table II.

IV. RESULTS AND DISCUSSIONS

A. Performance comparisons

In this subsection, two comparisons are first conducted to quantify the improvement by using GPR+ARD model for calendar aging prediction.

1) Comparisons of various kernel functions: To evaluate the performance of different kernel functions in the calendar aging prediction domain, four covariance functions including solo SE , solo M32, SE with ARD kernel (ARD+SE), and M32 with ARD kernel (ARD+M32), are compared with respect to their training and prediction performance. The initial values of all GPR models' hyperparameters are set through using MATLAB GPR toolbox, and defined as: for the solo SE and M32 kernels, $\sigma_{SE} = \sigma_{M32} = 0.1$, $l_{SE} = l_{M32} = 2$; for the ARD+SE and ARD+M32 kernels, $\sigma_{SE} = \sigma_{M32} = 0.1$, $l_T = l_{SOC} = 2$, $l_c = 1$. Here, Case 5 with the worst training results, and Case 6 with the largest one-step prediction errors, are specified for performance comparisons.
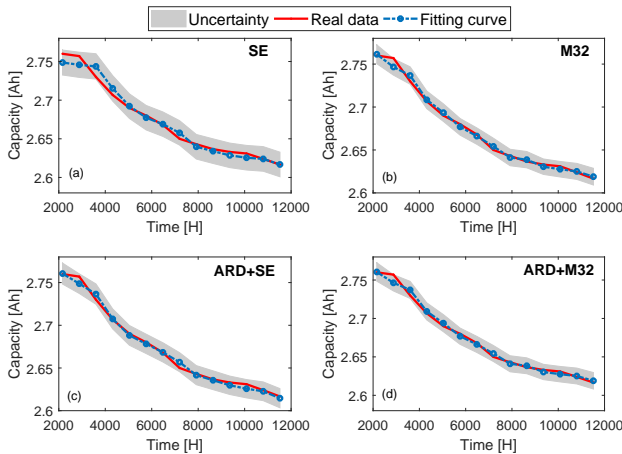

Fig. 6. Training results by using different kernel functions for Case 5 data.

Fig. 6 illustrates the training results by using different kernel functions for Case 5 data. It is evident that experimental capacity presents a non-linear declining trend during storage with 0.5 SOC and $25°C$ temperature. Although solo SE function can capture the overall degradation trend with the largest confidence range, some points are still mismatched especially at beginning. After modifying SE with the ARD structure, as shown in Fig. 6(c), the training performance can be effectively improved. Here the MAE for ARD+SE case is 0.0091, which is 33.1% less than that at solo SE case. For solo M32 and ARD+M32 kernels, it seems that better training results are obtained for both the cases. After using the ARD structure, the MAE for ARD+M32 case becomes 0.0078, which is 8.3% less than that of the solo M32 case. These satisfactory training results are mainly due to the variable length scales of the ARD structure. We can conclude that with the same calendar aging dataset, the training performance can be improved by using ARD-based kernel functions.

After training, the GPR models with different kernel functions are applied to predict the future capacity in different storage conditions. Fig. 7 and Table III illustrate the prediction
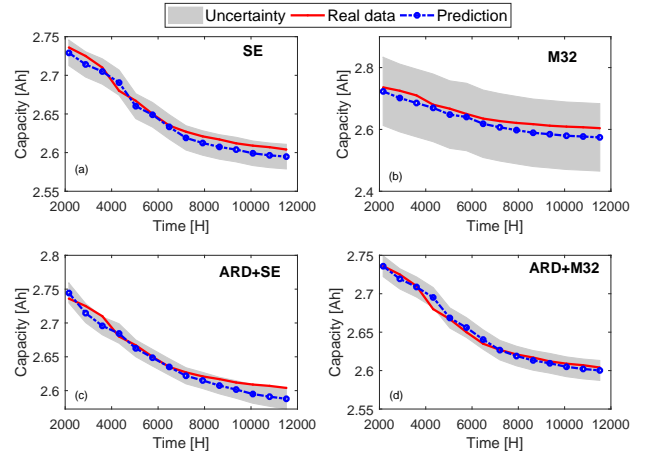

Fig. 7. Prediction results by using different kernel functions for Case 6 data.

TABLE III
PREDICTION QUANTITATIVE METRICS FOR DIFFERENT KERNELS

Kernel types.	solo SE	solo M32	ARD+SE	ARD+M32
MAE	0.0161	0.0300	0.0154	**0.0109**
RMSE	0.0100	0.0228	0.0082	**0.0054**
R^2	0.948	0.927	0.957	**0.978**
CS	0.929	1	0.929	**0.954**

results and the corresponding quantitative metrics for Case 6 data. It can be observed that by using solo SE kernel, although the obtained 95% confidence range almost covers the overall degradation trend, the mean prediction values still mismatch the real experimental data in most time points (here the CS and RMSE values are 0.929 and 0.0100, respectively). For solo M32 kernel, the prediction values are all lower than the actual values (here MAE, RMSE and R^2 become the worst ones as 0.0300, 0.0228, and 0.927, respectively). Besides, the corresponding 95% confidence range distributes in a wide region, implying that high uncertainty is achieved in this case. These prediction failures are mainly caused by the over-fitting problem, implying the poor generalization ability of solo kernel structure. In comparison, the predicted values get closer to the real capacity data by using the ARD-based SE kernel, indicating the effectiveness of ARD structure. But several mismatch points still exist especially after 8000h points for this case, which means the SE kernel cannot capture the overall capacity degradation dynamics. In Fig. 7(d), by using the ARD-based M32 kernel, the capacity trend is well captured as desired. Quantitatively, the RMSE for Case 6 data here is just 0.0054, which is 76.3% and 34.1% less than the solo M32 case and ARD+SE case, respectively. Besides, the 95% confidence range distributes in a narrow region for such a case, indicating a high credibility for the prediction results. These satisfactory performance is caused by the strong feature extraction abilities of ARD and high robustness of M32 kernel. Accordingly, ARD-based M32 kernel is selected for predicting calendar aging in the following studies.

2) Comparisons of training results for GPR and RCL models: Next, in order to further evaluate the effectiveness of the
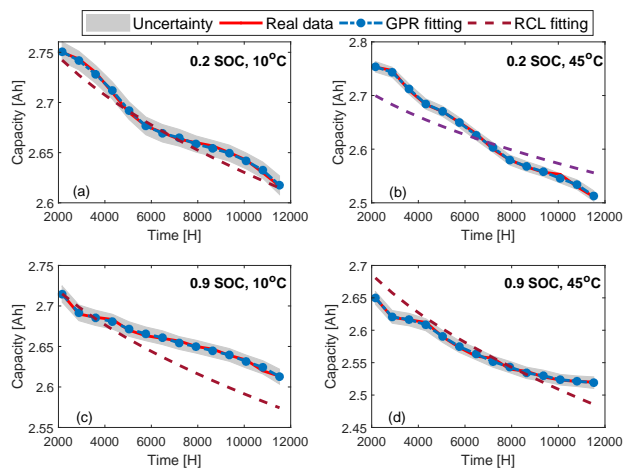
Fig. 8. Comparisons of training results by using GPR model and RCL model. (a) Case 1, (b) Case 3, (c) Case 7, and (d) Case 9.

Fig. 9. Prediction results by using full-data from 'Group 1' cases as the training set. (a) Case 2, (b) Case 4, (c) Case 6, and (d) Case 8.

TABLE IV
QUANTITATIVE TRAINING METRICS FOR GPR MODEL AND RCL MODEL

Case No.	Case 1	Case 3	Case 7	Case 9
MAE (RCL)	0.0214	0.0432	0.0463	0.0401
MAE (GPR)	0.0042	0.0041	0.0046	0.0029
RMSE (GPR)	0.0012	0.0010	0.0009	0.0008
CS (GPR)	0.954	0.954	0.954	0.954

TABLE V
PREDICTION QUANTITATIVE METRICS AFTER FULL-DATA TRAINING

Case No.	Case 2	Case 4	Case 6	Case 8
MAE	0.0115	0.0107	0.0122	0.0076
RMSE	0.0043	0.0051	0.0052	0.0046
R^2	0.981	0.985	0.978	0.988
CS	0.929	0.929	0.929	0.954

GPR model for calendar aging prediction, the RCL model is used as a comparison. Fig. 8 and Table IV illustrate the training results and the corresponding quantitative metrics for different storage conditions, respectively. It is worth noticing that the RCL model gives a general trend of capacity aging without the direct uncertainty quantification for the predicted values. Even for the best fitting results obtained under 0.2 SOC and $10°C$ storage temperature, the MAE is larger than those of GPR model, respectively. For the remaining three cases of 'Group 2' validation, the corresponding fitting results also present large differences with the measured data, implying that this RCL model is inadequate to capture capacity degradation of our dataset case. The main reason causes RCL model becomes bad would be the unrecorded initial capacity fading for such dataset. In comparison, by using the ARD-based GPR model, both the overall capacity decline trend and local nonlinear fluctuations are well fitted as desired. From Table IV, the MAE and RMSE for all cases by using GPR model are within 0.005 and 0.0012, respectively. Moreover, the CS values are all equal to 0.954, indicating the high training accuracy and good generalization ability by using our proposed GPR+ARD data-driven model.

B. Full-data training results of ARD+M32

Fig. 9 and Table V present the prediction results and the corresponding quantitative metrics for 'Group 2' cases after full-data training based on the 'Group 1' cases. It can be seen that the predicted capacity values for all cases match the actual data well. The trained ARD-based GPR model captures the overall capacity degradation trends well as the RMSE of
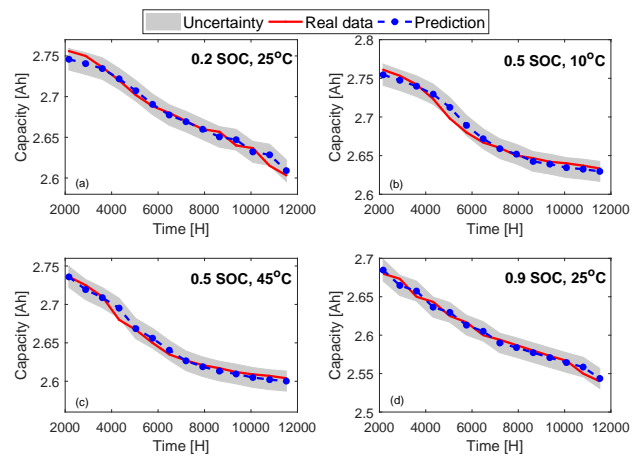
all predicted samples are less than 0.006. Besides, among all samples, the maximum MAE value is 0.0122, obtained for Case 6 data. This is mainly caused by the insufficient training data as only Case 5 covers 0.5 SOC condition. However, this MAE is still less than 0.5% capacity range, indicating that high accuracy is also achieved for such a case. For Case 8 with 0.9 SOC and $25°C$ storage temperature, the corresponding CS value reaches 0.954, which means that the actual results are all covered within the obtained confidence range. Interestingly, CS values for other cases are all 0.929, implying that the corresponding confidence ranges are also reliable. Therefore, it can be concluded that the full-data trained GPR model with ARD structure is effective and highly accurate for battery calendar aging prediction under various storage conditions.

C. Partial-data training results

For GPR technique, the inclusion of a larger number of relevant data could lead to explain the data better and learn more underlying mapping information, further resulting in more accurate prediction results, and narrower confidence boundaries. However, collecting calendar aging data under various storage conditions is an extremely time-consuming process in real-world applications. In such a case, it is meaningful to develop a reliable model with a satisfactory accuracy level based on partial training data. To evaluate the partial-data training results and the corresponding prediction performance of the proposed ARD-based GPR model, the capacity data before 8000h of all 'Group 1' cases (nearly 7/3 split) are chosen as the dataset for the training part, while the remaining data are employed as the validation set.
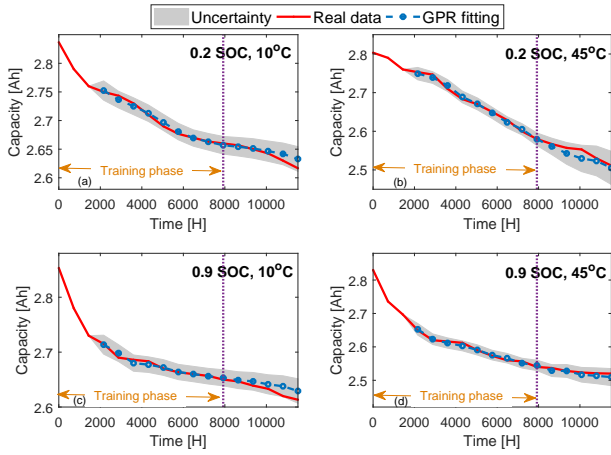
Fig. 10. Training results by using partial-data from 'Group 1' cases as the training set. (a) Case 1, (b) Case 3, (c) Case 7, and (d) Case 9.

Fig. 10 illustrates the results for 'Group 1' cases based on the partial-data training. From Fig. 10, it is observed that for various cases with different storage conditions, the capacity values are highly similar to the real data in training phase, indicating that an accurate fitting result is obtained for our GPR model. After 8000h, apart from Case 9 that still presents the highly similar trend with just 0.0032 MAE, other cases all show more or less differences. Specifically, Case 1 and Case 7 obtain the MAE values of 0.0116 and 0.0154 at both 11520h, respectively. Case 3 achieves 0.0123 MAE at 10800h. It therefore proves that decreasing the training data will result in the information loss of capacity fade in calendar aging, further reducing the extrapolation and generalization performance of the trained-model. Even so, by using the GPR model with the ARD structure, all MAE values are still less than 0.5% capacity range, which means that the training results are still reliable. To further evaluate the prediction results of partial-data training, all data from 'Group 2' cases are then employed as the validation set.
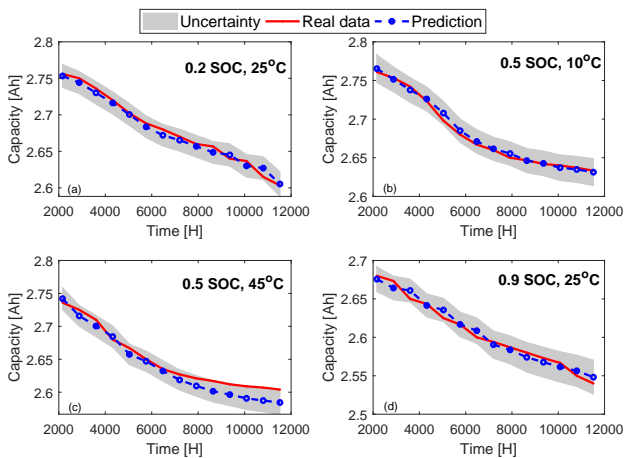

Fig. 11. Prediction results by using partial-data from 'Group 1' cases as the training set. (a) Case 2, (b) Case 4, (c) Case 6, and (d) Case 8.

After training the GPR model based on the partial-data from

TABLE VI
PREDICTION QUANTITATIVE METRICS AFTER PARTIAL-DATA TRAINING

Case No.	Case 2	Case 4	Case 6	Case 8
MAE	0.0128	0.0112	0.0167	0.0118
RMSE	0.0065	0.0057	0.0084	0.0061
R^2	0.964	0.979	0.959	0.972
CS	0.929	0.929	0.896	0.954

'Group 1' cases, the prediction results for 'Group 2' cases are presented in Fig. 11. Moreover, detailed quantitative metrics are examined in Table VI. It is seen that Case 4 presents much higher accuracy in the whole validation process with the smallest values of MAE (0.0112) and RMSE (0.0057), respectively. For Case 2, the corresponding RMSE is 0.0065, indicating that satisfactory overall capacity prediction is also achieved. Here the MAE is 0.0128, caused by a short-period mismatch around 11000h. From Fig 11(d), the predicted values present more fluctuations in comparison with those in the full-data training case. Quantitatively, here the MAE and RMSE for Case 8 become 0.0118 (55.3% increase) and 0.0061 (32.6% increase). Even so, the result of Case 8 still presents a satisfactory capacity prediction. In comparison, Case 6 has the worst prediction due to several mismatches occurring after 7000h. The RMSE for Case 6 reaches 0.0084, which is 61.5% more than that under the full-data training. This result is reasonable due to the decreased capacity characteristics covered by using partial data training. However, the MAE for Case 6 is still less than 0.6% capacity range (here is 0.0167), which means that the corresponding predicted accuracy is also acceptable. Besides, the CS values for all cases are all larger than 0.896, implying that the confidence levels are reliable. In conclusion, these facts signify that with a suitable partial-data training, the proposed GPR model is also capable of excavating the useful information, therefore providing reliable and accurate prediction results for calendar aging under various conditions.

D. Multi-step calendar aging prediction

Multi-step calendar aging prediction is more meaningful in real-world applications as it can provide the entire future trend of capacity degradation. To evaluate the multi-step prediction performance of our proposed ARD-based GPR model, a multi-step prediction test is conducted for all 'Group 2' cases in comparison with the RCL model.

TABLE VII
QUANTITATIVE METRICS FOR MULTI-STEP PREDICTION

Case No.	Case 2	Case 4	Case 6	Case 8
MAE (RCL)	0.0223	0.0167	0.0472	0.0413
MAE (GPR)	0.0132	0.0148	0.0152	0.0124
RMSE (GPR)	0.0073	0.0102	0.0104	0.0069
R^2 (GPR)	0.961	0.946	0.943	0.970
CS (GPR)	0.954	0.911	0.907	0.954

In this test, after obtaining a new predicted capacity value by our GPR+ARD model, a recursive process is iteratively conducted to predict future capacity until the last one is achieved. It should be known that due to the structure as illustrated
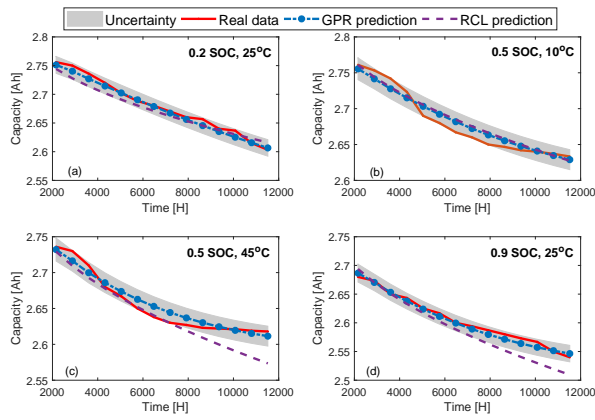
Fig. 12. Multi-step calendar aging prediction results of ARD-GPR model and RCL model. (a) Case 2, (b) Case 4, (c) Case 6, and (d) Case 8.

in Fig. 5, ARD+GPR model requires the information of first $k+1$ historical capacity points ($k = 2$ in our study), while the RCL model just requires the initial one capacity point. Here the comparison between two models is conducted after the $k+1$th capacity points. Fig. 12 and Table VII illustrate the multi-step prediction results and the corresponding quantitative metrics for both RCL and GPR+ARD models, respectively. From Fig. 12, it can be observed that relatively large predicted mismatches exist for cases by using the RCL model (here the worst MAE reaches 0.0472 for Case 6 at 11520 h), indicating the poor generalization ability of the RCL model for our dataset. In comparison, by using the GPR+ARD model, although several mismatches occur especially in large local fluctuations of Case 4 and Case 6, the entire capacity decline trends are still captured reliably for all cases. These increased local mismatches are reasonable as the predicted errors are accumulated for multi-step conditions. Here the RMSE for Case 4 and Case 6 become 0.0102 and 0.0104, which are nearly twice larger than those of one-step prediction cases. These results are mainly caused by the poor training dataset for 0.5 SOC condition (just Case 5 owns the information of 0.5 SOC). However, the worst MAE is still within 0.7% capacity range (here is 0.0152 for Case 6), indicating that the corresponding multi-step prediction results are acceptable for all cases. Moreover, all the obtained uncertainty ranges cover the local fluctuations. It can be concluded that even for the multi-step prediction, the developed GPR+ARD model can capture the overall capacity degradation trends well with an acceptable confidence level.

E. Prediction at new condition through accelerated aging data training

In the real world, batteries experience a wide range of storage temperatures and SOCs. Developing a lifetime model based on converting accelerated aging data to predict new degradation case is another promising research topic [32], [36]. To evaluate the corresponding performance of proposed GPR+ARD model, a test regarding the entirely new condition prediction is conducted in this subsection.
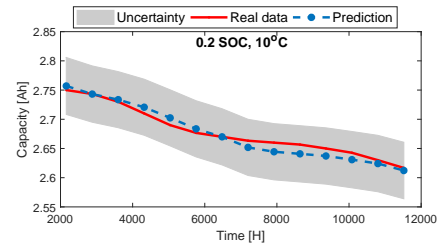

Fig. 13. Prediction result of Case 1 through training based on the accelerated aging data.

TABLE VIII
QUANTITATIVE METRICS AFTER ACCELERATED AGING TRAINING

Case No.	Case 5	Case 6	Case 8	Case 9	**Case 1**
MAE	0.0066	0.0082	0.0074	0.0089	0.0162
RMSE	0.0027	0.0035	0.0031	0.0037	0.0106
R^2	0.989	0.978	0.983	0.975	0.942
CS	0.954	0.954	0.954	0.929	1

In this test, GPR+ARD model is trained through using accelerated aging data. Specifically, the aging data under the relatively high SOCs and temperatures from Case 5, Case 6, Case 8 and Case 9 are utilized for model training. After that, data from Case 1 that represents an entirely new storage condition are used for validating our proposed model. Fig. 13 and Table VIII illustrate the prediction results of Case 1 after accelerated aging data training and the corresponding quantitative metrics, respectively. One obvious observation is that the obtained uncertainty bounds become relatively wider than the tests from previous subsections. This is hardly surprising given that temperature and SOC in Case 1 are both different from the utilized accelerated aging data. In such situations, the covariance values calculated by the kernel function are smaller, leading to the broader confidence boundaries. However, it is clear that these uncertainty bounds still cover the real data. The overall capacity degradation trend of Case 1 can be captured by the predicted capacity values, indicating that the proposed GPR+ARD model also presents effectiveness for such a case.

F. Further Discussions

Due to the lack of exploiting machine learning-based approaches for calendar aging prediction in the existing published work, for the first time, this article focuses especially on the development of the GPR technique with ARD kernel to achieve satisfactory capacity prediction under various storage conditions. In the study, the calendar aging dataset is acquired from an OEM automotive company with some initial degradation due to the reduced begin of life (BOL) capacity of the battery. Then the observed trends would inevitably decrease the prediction performance of the utilized RCL model, while favouring the step-by-step GPR model. Based upon our test results, several useful observations can be made: 1) in order to take full advantage of the semi-empirical model, a well-designed aging test that covers the battery's nominal capacity and considers overhang effects is recommended [28]. 2) in real-world applications, missing data related to any usage and subsequent degradation of a cell is a practical and

likely scenario to occur. In such circumstances, our proposed GPR+ARD model outperforms the RCL model with regards to prediction performance and uncertainty quantification. 3) to avoid under-fitting problem of pure data-driven technique, a dataset covering enough useful information is suggested in the training phase [14], [30]. Future work could include an effective combination of the proposed GPR technique with battery electrochemical knowledge or electrothermal models, and the performance improvements in research areas such as the conversion of accelerated aging data to predict entirely new degradation cases, the holistic aging predictions regarding both calendar and cycling modes.

V. CONCLUSION

In this paper, effective capacity prognosis under various storage conditions for Li-ion batteries is presented. The GPR technique with ARD kernel is employed to synthesize a data-driven model for battery calendar aging prediction. Based upon the GPR toolbox of Matlab 2018 with a 2.40 GHz Intel Pentium 4 CPU, our proposed GPR model can be well-trained within 10s. Illustrative results corroborate that the ARD+M32 kernel outperforms other kernels in both training and validation processes (here the MAE and RMSE are less than 0.011 and 0.0055 for all cases). Based upon our measured dataset, such GPR model exhibits improved prediction performance with higher accuracy and better generalization ability. Moreover, the uncertainty level of predicted results can be considered simultaneously. Even for the partial-data training test, multi-step prediction test and accelerated aging training test, the predicted results are satisfactory in terms of the accuracy (here the worst RMSE are less than 0.0105) and the reliable confidence range for various storage conditions. Without any mechanism knowledge, it is worth noting that the proposed model can be easily extended to other battery types for resilient calendar aging prognosis.

REFERENCES

[1] X. Hu, D. Cao, and B. Egardt, "Condition monitoring in advanced battery management systems: moving horizon estimation using a reduced electrochemical model," *IEEE/ASME Transactions on Mechatronics*, vol. 23, no. 1, pp. 167–178, 2018.

[2] S. Grolleau, A. Delaille, H. Gualous, P. Gyan, R. Revel, J. Bernard, E. Redondo-Iglesias, J. Peter, and S. Network, "Calendar aging of commercial graphite/LiFePO$_4$ cell–predicting capacity fade under time dependent storage conditions," *Journal of Power Sources*, vol. 255, pp. 450–458, 2014.

[3] M. Dubarry, N. Qin, and P. Brooker, "Calendar aging of commercial li-ion cells of different chemistries–a review," *Current Opinion in Electrochemistry*, 2018.

[4] S. S. Zhang, "A review on electrolyte additives for lithium-ion batteries," *Journal of Power Sources*, vol. 162, no. 2, pp. 1379–1394, 2006.

[5] L. Su, J. Zhang, J. Huang, H. Ge, Z. Li, F. Xie, and B. Y. Liaw, "Path dependence of lithium ion cells aging under storage conditions," *Journal of Power Sources*, vol. 315, pp. 35–46, 2016.

[6] M. Ecker, N. Nieto, S. Käbitz, J. Schmalstieg, H. Blanke, A. Warnecke, and D. U. Sauer, "Calendar and cycle life study of Li(NiMnCo)O$_2$-based 18650 lithium-ion batteries," *Journal of Power Sources*, vol. 248, pp. 839–851, 2014.

[7] H. Ekström and G. Lindbergh, "A model for predicting capacity fade due to sei formation in a commercial graphite/LiFePO$_4$ cell," *Journal of The Electrochemical Society*, vol. 162, no. 6, pp. A1003–A1007, 2015.

[8] K. L. Gering, "Novel method for evaluation and prediction of capacity loss metrics in li-ion electrochemical cells," *Electrochimica Acta*, vol. 228, pp. 636–651, 2017.

[9] J. Schmalstieg, S. Käbitz, M. Ecker, and D. U. Sauer, "A holistic aging model for Li(NiMnCo)O$_2$ based 18650 lithium-ion batteries," *Journal of Power Sources*, vol. 257, pp. 325–334, 2014.

[10] M. Petit, E. Prada, and V. Sauvant-Moynot, "Development of an empirical aging model for li-ion batteries and application to assess the impact of vehicle-to-grid strategies on battery lifetime," *Applied Energy*, vol. 172, pp. 398–407, 2016.

[11] E. Redondo-Iglesias, P. Venet, and S. Pelissier, "Eyring acceleration model for predicting calendar ageing of lithium-ion batteries," *Journal of Energy Storage*, vol. 13, pp. 176–183, 2017.

[12] J. de Hoog, J.-M. Timmermans, D. Ioan-Stroe, M. Swierczynski, J. Jaguemont, S. Goutam, N. Omar, J. Van Mierlo, and P. Van Den Bossche, "Combined cycling and calendar capacity fade modeling of a nickel-manganese-cobalt oxide cell with real-life profile validation," *Applied Energy*, vol. 200, pp. 47–61, 2017.

[13] S. L. Hahn, M. Storch, R. Swaminathan, B. Obry, J. Bandlow, and K. P. Birke, "Quantitative validation of calendar aging models for lithium-ion batteries," *Journal of Power Sources*, vol. 400, pp. 402–414, 2018.

[14] M. Lucu, E. Martinez-Laserna, I. Gandiaga, and H. Camblong, "A critical review on self-adaptive li-ion battery ageing models," *Journal of Power Sources*, vol. 401, pp. 85–101, 2018.

[15] D. Yang, Y. Wang, R. Pan, R. Chen, and Z. Chen, "State-of-health estimation for the lithium-ion battery based on support vector regression," *Applied Energy*, vol. 227, pp. 273–283, 2018.

[16] J. Wei, G. Dong, and Z. Chen, "Remaining useful life prediction and state of health diagnosis for lithium-ion batteries using particle filter and support vector regression," *IEEE Transactions on Industrial Electronics*, vol. 65, no. 7, pp. 5634–5643, 2018.

[17] X. Hu, J. Jiang, D. Cao, and B. Egardt, "Battery health prognosis for electric vehicles using sample entropy and sparse bayesian predictive modeling," *IEEE Transactions on Industrial Electronics*, vol. 63, no. 4, pp. 2645–2656, 2016.

[18] C. Hu, H. Ye, G. Jain, and C. Schmidt, "Remaining useful life assessment of lithium-ion batteries in implantable medical devices," *Journal of Power Sources*, vol. 375, pp. 118–130, 2018.

[19] C. Sbarufatti, M. Corbetta, M. Giglio, and F. Cadini, "Adaptive prognosis of lithium-ion batteries based on the combination of particle filters and radial basis function neural networks," *Journal of Power Sources*, vol. 344, pp. 128–140, 2017.

[20] G.-W. You, S. Park, and D. Oh, "Diagnosis of electric vehicle batteries using recurrent neural networks," *IEEE Transactions on Industrial Electronics*, vol. 64, no. 6, pp. 4885–4893, 2017.

[21] Y. Zhang, R. Xiong, H. He, and M. Pecht, "Long short-term memory recurrent neural network for remaining useful life prediction of lithium-ion batteries," *IEEE Transactions on Vehicular Technology*, 2018.

[22] M. H. Lipu, M. Hannan, A. Hussain, M. Hoque, P. J. Ker, M. Saad, and A. Ayob, "A review of state of health and remaining useful life estimation methods for lithium-ion battery in electric vehicles: Challenges and recommendations," *Journal of Cleaner Production*, 2018.

[23] K. Liu, K. Li, Q. Peng, and C. Zhang, "A brief review on key technologies in the battery management system of electric vehicles," *Frontiers of Mechanical Engineering*, vol. 14, no. 1, pp. 47–64, 2019.

[24] R. R. Richardson, C. R. Birkl, M. A. Osborne, and D. Howey, "Gaussian process regression for in-situ capacity estimation of lithium-ion batteries," *IEEE Transactions on Industrial Informatics*, 2018.

[25] G. O. Sahinoglu, M. Pajovic, Z. Sahinoglu, Y. Wang, P. V. Orlik, and T. Wada, "Battery state-of-charge estimation based on regular/recurrent gaussian process regression," *IEEE Transactions on Industrial Electronics*, vol. 65, no. 5, pp. 4311–4321, 2018.

[26] D. Yang, X. Zhang, R. Pan, Y. Wang, and Z. Chen, "A novel gaussian process regression model for state-of-health estimation of lithium-ion battery using charging curve," *Journal of Power Sources*, vol. 384, pp. 387–395, 2018.

[27] P. Keil, "Aging of lithium-ion batteries in electric vehicles," Ph.D. dissertation, Technische Universität München, 2017.

[28] M. Lewerenz, G. Fuchs, L. Becker, and D. U. Sauer, "Irreversible calendar aging and quantification of the reversible capacity loss caused by anode overhang," *Journal of Energy Storage*, vol. 18, pp. 149–159, 2018.

[29] B. Gyenes, D. Stevens, V. Chevrier, and J. Dahn, "Understanding anomalous behavior in coulombic efficiency measurements on li-ion batteries," *Journal of The Electrochemical Society*, vol. 162, no. 3, pp. A278–A283, 2015.

[30] C. K. Williams and C. E. Rasmussen, *Gaussian processes for machine learning*, vol. 2, no. 3. MIT Press Cambridge, MA, 2006.

[31] K. Liu, K. Li, Q. Peng, Y. Guo, and L. Zhang, "Data-driven hybrid internal temperature estimation approach for battery thermal management," *Complexity*, vol. 2018, 2018.

[32] M. Ecker, J. B. Gerschler, J. Vogel, S. Käbitz, F. Hust, P. Dechent, and D. U. Sauer, "Development of a lifetime prediction model for lithium-ion batteries based on extended accelerated aging test data," *Journal of Power Sources*, vol. 215, pp. 248–257, 2012.

[33] R. R. Richardson, M. A. Osborne, and D. A. Howey, "Gaussian process regression for forecasting battery state of health," *Journal of Power Sources*, vol. 357, pp. 209–219, 2017.

[34] J. Zhao, L. Chen, W. Pedrycz, and W. Wang, "Variational inference based automatic relevance determination kernel for embedded feature selection of noisy industrial data," *IEEE Transactions on Industrial Electronics*, 2018.

[35] K. Liu, C. Zou, K. Li, and T. Wik, "Charging pattern optimization for lithium-ion batteries with an electrothermal-aging model," *IEEE Transactions on Industrial Informatics*, vol. 14, no. 12, pp. 5463–5474, 2018.

[36] D.-I. Stroe, M. Świerczyński, A.-I. Stan, R. Teodorescu, and S. J. Andreasen, "Accelerated lifetime testing methodology for lifetime estimation of lithium-ion batteries used in augmented wind power plants," *IEEE Transactions on Industry Applications*, vol. 50, no. 6, pp. 4006–4017, 2014.

Xiaosong Hu (SM'16) received the PhD degree in Automotive Engineering from Beijing Institute of Technology, China, in 2012. He did scientific research and completed the PhD. dissertation in Automotive Research Center at the University of Michigan, Ann Arbor, USA, between 2010 and 2012.

He is currently a professor at the State Key Laboratory of Mechanical Transmissions and at the Department of Automotive Engineering, Chongqing University, Chongqing, China. He was a postdoctoral researcher at the Department of Civil and Environmental Engineering, University of California, Berkeley, USA, between 2014 and 2015, as well as at the Swedish Hybrid Vehicle Center and the Department of Signals and Systems at Chalmers University of Technology, Gothenburg, Sweden, between 2012 and 2014. He was also a visiting postdoctoral researcher in the Institute for Dynamic systems and Control at Swiss Federal Institute of Technology (ETH), Zurich, Switzerland, in 2014. His research interests include battery management technologies and modeling and controls of electrified vehicles.

Dr. Hu has published more than 100 high-caliber journal/conference papers. He has been a recipient of several prestigious awards/honors, including SAE Ralph Teetor Educational Award in 2019, Emerging Sustainability Leaders Award in 2016, EU Marie Currie Fellowship in 2015, ASME DSCD Energy Systems Best Paper Award in 2015, and Beijing Best PhD Dissertation Award in 2013. He is a Senior Member of IEEE.

Kailong Liu (M'18) is a Research Fellow in the Warwick Manufacturing Group, University of Warwick, United Kingdom. He received the B.Eng. degree in electrical engineering and the M.Sc. degree in control theory and control engineering from Shanghai University, China, and the Ph.D. degree in electrical engineering from the Energy, Power and Intelligent Control group, Queen's University Belfast, United Kingdom, in 2011, 2014, and 2018, respectively.

He was a Visiting Student Researcher at the Tsinghua University and the North China Electric Power University, China, in 2016. His research interests include modeling, optimization and control with applications to electrical/hybrid vehicles, energy storage, and battery management system.
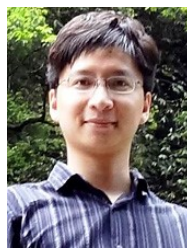
Dr. Liu was the student chair of IEEE QUB student branch and a recipient of awards such as EPSRC Scholarship, Santander International Scholarship, and QUB ESM International Scholarship.

Mattin Lucu received his M.Sc in Integration of Renewable Energy Sources into the Electricity Grid from the University of the Basque Country, UPV-EHU (Spain) in 2016. During his graduate studies, he worked as R&D intern successively at EneR-GEA research group (ESTIA Engineering School, France) in wind turbine emulation and control, and at EDP in the analysis of photovoltaic power insertion in low-voltage distribution networks. In 2016, he joined the IK4-Ikerlan Technology Research Centre, where he is coursing a Ph.D. degree in collaboration with the University of the Basque Country.

His research interests include electrochemical energy storage systems and machine learning algorithms applied to their lifetime estimation.

Y i Li is a senior research associate at Lancaster University in the UK. Her research interests lie in Li-ion battery ageing mechanism identification, state of health estimation and lifetime prediction.
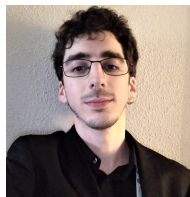
She received the B.E. degree in chemical engineering from the Easy China University of Science and Technology, China, in 2008; the M.S. degree in material science from Technical University of Munich, Munich, Germany in 2012; and the Ph.D degree in electrical engineering from the Vrije Universiteit Brussels, Brussels, Belgium in 2019.

Dhammika Widanalage is an Assistant Professor in modelling and energy storage at WMG, Warwick University and was the recipient of the WMG Early Career Researcher of the Year award in 2016. His research is in system identification theory, applied across several applications including batteries.

He leads the battery modelling research in the department and recently secured funding to lead the modelling activity as a PI (for WMG) on the Faraday Multiscale Modelling project, as a Co-I on the EPSRC Prosperity Partnership with Jaguar Land Rover and a PI and Co-I on four Innovate UK projects (PI and three Co-I). He is a member of the European Materials Modelling Community Interoperability and Repository Advisory Group (EMMC-IRAG) and supported the compilation of the Materials modelling-Terminology, Classification and Metadata document which is now publicly available to increase the use of material modelling with industrial end-users.